

Colloidal trains

Mahla Mirzaee-Kakhki¹, Adrian Ernst¹, Daniel de las Heras², Maciej Urbaniak³,
Feliks Stobiecki³, Andreea Tomita⁴, Rico Huhnstock⁴, Iris Koch⁴, Jendrik Gördes⁴,
Arno Ehresmann⁴, Dennis Holzinger⁴, Meike Reginka⁴, and Thomas M. Fischer^{1*}

¹ *Experimentalphysik X, Physikalisches Institut, Universität Bayreuth, D-95440 Bayreuth, Germany.*

² *Theoretische Physik II, Physikalisches Institut, Universität Bayreuth, D-95440 Bayreuth, Germany.*

³ *Institute of Molecular Physics, Polish Academy of Sciences, 60-179 Poznań, Poland.*

⁴ *Institute of Physics and Center for Interdisciplinary Nanostructure Science and Technology (CINaT), University of Kassel, D-34132 Kassel, Germany*

(Dated: November 18, 2019)

Single and double paramagnetic colloidal particles are placed above a magnetic square pattern and are driven with an external magnetic field precessing around a high symmetry direction of the pattern. The external magnetic field and that of the pattern confine the colloids into lanes parallel to a lattice vector of the pattern. The precession of the external field causes traveling minima of the magnetic potential along the direction of the lanes. At sufficiently high frequencies of modulation only the doublets respond to the external field and move in direction of the traveling minima along the lanes, while the single colloids cannot follow and remain static. We show how the doublets can induce a coordinated motion of the single colloids building colloidal trains made of a chain of several single colloids transported by doublets.

Biomimetics is used to implement biological functions to artificial devices, fulfilling tasks in a non biological environment. Well known examples are artificial swimmers [1–3] and active systems [4] that can be used to e.g. transport a load. Microscopic dynamics can also be inspired by large scale transport systems such as trains. A railroad train is powered either by a separate locomotive or by multiple units of self propelled equally powered carriages. In nature the motility of family members of animals trailing behind each other is neither concentrated in the animal heading the trail nor is it distributed equally amongst family members. Young goslings trailing behind one of their parents need less but not zero power to follow their more powerful mother goose [5]. When elephants travel they walk in a line placing their youngest in between the grownups with a grownup at the head and at the tail. In the spirit of other bioinspired magnetic colloidal dynamics [1–3, 6, 7] we generate a biomimetic train of a collective ensemble of paramagnetic colloids. Single colloids are too weak to move on their own along the line and must be assisted to move by pushing of the train with a larger paramagnetic colloidal doublet. The train is confined to an effectively one dimensional lane created via a colloidal potential which is generated by the combination of a magnetic square pattern and an external magnetic field. The power of each unit in the train is generated by modulating the external field on a control loop. Colloidal trains can only move above a square lattice if a sufficiently flat potential valley is created by orienting the external field roughly in direction of a primitive unit vector of the square magnetic pattern.

We illustrate the doublet assisted motion of a train of single colloids using a square magnetic lattice [8, 9], Fig. 1(a). In the experiments, single paramagnetic colloidal particles or doublets of particles move on a plane

above a thin Co/Au layered system with perpendicular magnetic anisotropy lithographically patterned via ion bombardment [9–11]. The pattern is a square lattice of magnetized domains with a mesoscopic pattern lattice constant $a \approx 7 \mu\text{m}$, see a sketch in Fig. 1(a). The pattern is magnetized in the $\pm\mathbf{z}$ -direction, normal to the film. The pattern is spin coated with a $1.6 \mu\text{m}$ polymer film that serves as a spacer between pattern and the colloids. The paramagnetic colloidal particles (diameter $2.8 \mu\text{m}$) are immersed in water. A uniform time-dependent external magnetic field \mathbf{H}_{ext} of constant magnitude ($H_{\text{ext}} = 4 \text{kAm}^{-1}$) is superimposed to the non-uniform and time-independent magnetic field generated by the pattern \mathbf{H}_p ($H_p \approx 1 \text{kAm}^{-1}$). The external field is strong enough such that some of the paramagnetic particles self-assemble into doublets due to induced dipolar interactions between the single colloidal particles. The doublets then align with the direction of the external field. Our control space \mathcal{C} is the surface of a sphere that represents all possible orientations of the external field. We vary the external field $\mathbf{H}_{\text{ext}}(t)$ with time t performing periodic closed modulation loops in \mathcal{C} .

Both \mathbf{H}_p and \mathbf{H}_{ext} create a potential $U \propto -\mathbf{H}_{\text{ext}} \cdot \mathbf{H}_p$. The potential is a periodic function of the position of the colloids in the magnetic lattice and it depends parametrically on the orientation of the external field in control space \mathcal{C} . At every time during the modulation loop, the colloids are attracted toward the minima of the potential. Full details about the computation of U and the motion of single colloids are given in Refs. [8, 9]. Here, we briefly explain the points relevant for the present study. For a square lattice, there exist four special points (fence points) in \mathcal{C} . The four points represent four directions of \mathbf{H}_{ext} which are parallel and antiparallel to the lattice vectors of the square pattern. If the modulation loop

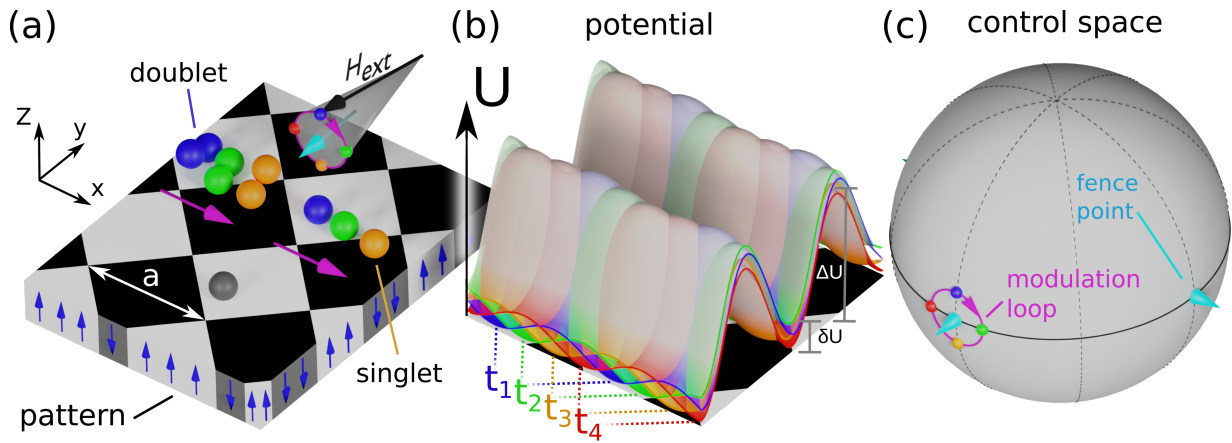


FIG. 1: Schematic of the setup. (a) Single and double spherical colloidal particles are placed on top of a lithographic magnetic square pattern (lattice constant $a \approx 7 \mu\text{m}$) of up (white) and down (black) magnetized domains along the \mathbf{z} -axis. An isolated single colloid (gray) does not move at the modulation frequency applied in the experiments. Doublets are able to respond to the external field and can also induce motion of single colloids. The color (blue, green, and orange) of the doublet and of the singlet represents the position at three different times (t_1, t_2 , and t_3) during the modulation loop. (b) Magnetic potential U created by the pattern and the external potential for four different times ($t_i, i = 1, 2, 3, 4$) during one modulation loop (red, blue, green, and orange) of the external field. The ratio between the large and the small barriers of the potential is $\Delta U/\delta U \approx 10$. (c) Each point in control space \mathcal{C} (gray sphere) corresponds to a different orientation of the external field. The experimental modulation loop is highlighted in purple. The loop winds around a fence point (cyan) of control space. The colors of the four potentials in (b) and the coloring of the moving colloidal positions (a) correspond to the four colored points on the loop in control space.

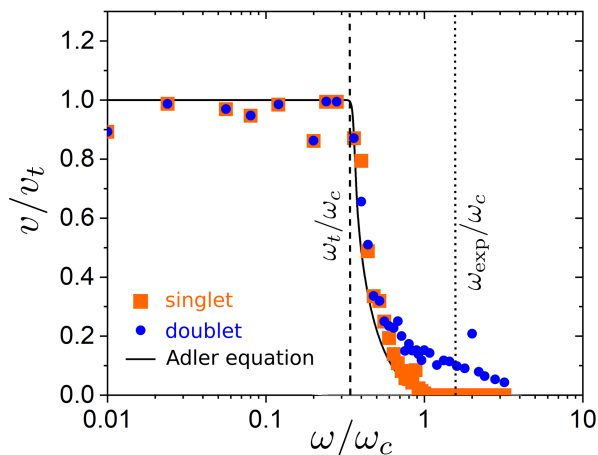


FIG. 2: Scaled magnitude of the velocity of singlets (orange squares) and doublets (blue circles) as a function of the scaled driving frequency. The black solid line is a fit of the singlet velocity using the generalized Adler equation (1). The vertical lines indicate the scaled experimental frequency ω_{ext} and the topological frequency ω_t below which the motion is topologically protected.

of \mathbf{H}_{ext} in \mathcal{C} winds around one of the fence points, then the minima of the potential move one unit cell above the square pattern [8, 9]. The motion is topologically protected, with the set of winding numbers around the fence points defining the topological invariants.

If \mathbf{H}_{ext} points in the direction of a fence point, the magnetic potential U is effectively one-dimensional with

valleys along the direction perpendicular to \mathbf{H}_{ext} . For example, let the lattice vectors of the magnetic pattern point along \mathbf{x} and \mathbf{y} , Fig. 1(a). The magnetic potential U exhibits deep valleys along \mathbf{x} , Fig. 1(b), when \mathbf{H}_{ext} points along $-\mathbf{y}$, Fig. 1(c). If \mathbf{H}_{ext} slightly deviates from the direction of a fence point, see modulation loop in Fig. 1(c), then secondary minima of U appear along the direction of the valleys, Fig. 1(b). The variation of the potential along the valley δU is much smaller than in the transversal direction ΔU . In our experimental setup, we find $\Delta U/\delta U \approx 10$. Modulating the external field directions along a loop that encloses a fence point, Fig. 1(c), causes the minima of U to travel by one unit vector of the lattice upon completion of the loop. The frequency of the loop ω can be chosen such that single colloids cannot follow the potential minimum on their own but doublets move in direction of the traveling minima. If a doublet is on a collision course with a single colloid, then the doublet can render the single colloid mobile and drive it through the potential valley, Fig. 1(a).

In Fig. 2 we plot the speed of an isolated single colloid and that of an isolated doublet versus the driving angular frequency ω of the modulation loop in \mathcal{C} . At low frequencies, lower than the topological critical frequency ω_t , the motion is adiabatic and topologically protected. Singlets and doublets follow the potential minimum at all times. Hence, the displacement caused by a loop is topologically locked to the primitive lattice vector and particles move at the topological speed given by the lattice constant a times the frequency, i.e., $v_t = \omega a/2\pi$. However,

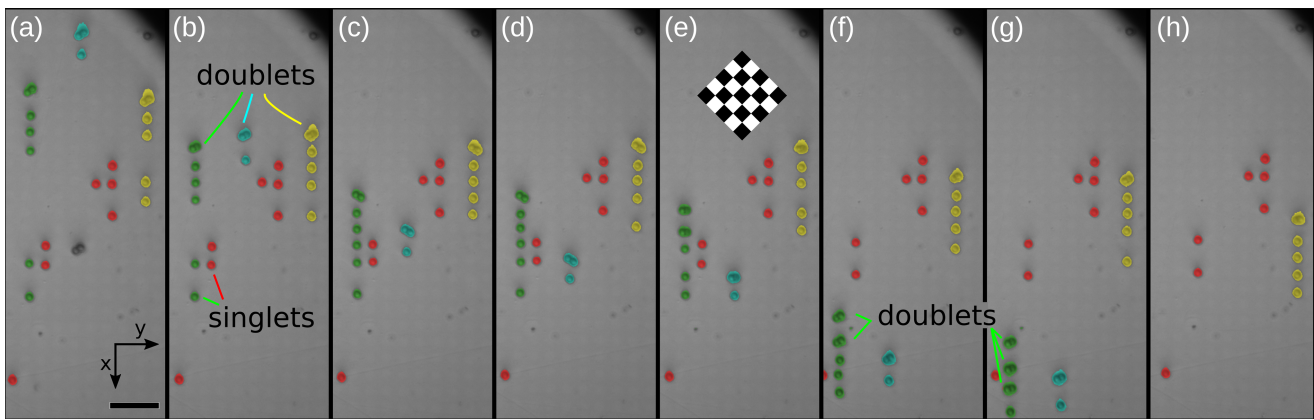


FIG. 3: Time sequence of microscope images of the pattern illustrating the motion of colloidal trains. Each train has been artificially colored differently. The images correspond to the times (a) $t = 0$ s, (b) $t = 8$ s, (c) $t = 13$ s (d) $t = 15$ s (e) $t = 17$ s (f) $t = 23$ s (g) $t = 25$ s and (h) $t = 30$ s. The period of one modulation loop is $2\pi/\omega_{\text{exp}} \approx 0.12$ s. Scale bar is $20 \mu\text{m}$. A sketch of the pattern has been superimposed in (e). A video clip recorded at twenty frames per second showing the motion of trains and the non motion of singlets is provided in the supplemental material (adfig3a.mp4). A second video clip (adfig3b.mp4) recorded at sixty frames per second shows a time-resolved slow motion of the doublet during the course of a few modulation loops.

at higher frequencies $\omega > \omega_t$ the speed drops below v_t , mostly due to viscous and adhesive forces impeding the motion. For singlets, the speed decreases with increasing frequency until the critical frequency ω_c is reached. At ω_c the isolated single colloids stop moving. The speed of the singlets is well described by a generalized Adler equation [12]

$$v/v_t = \begin{cases} 1 & \text{if } \omega \leq \omega_t \\ 1 - \sqrt{\frac{(\omega - \omega_t)((\omega_c - \omega)\omega_t + \omega\omega_c)}{(\omega_c - \omega_t)\omega^2}} & \text{if } \omega_t < \omega < \omega_c \\ 0 & \text{if } \omega \geq \omega_c \end{cases} \quad (1)$$

The force due to the potential acting on a doublet is roughly twice the force acting on a single colloidal particle. The viscous friction on the doublet, however, is less than twice the friction of a single colloid because of hydrodynamic interactions [13]. Hence, the doublet can still move at frequencies higher than the critical frequency of the singlets, and we have a regime where the doublet moves while the singlet is at rest. The experiments are performed at an angular frequency of $\omega \approx 52 \text{ s}^{-1} > \omega_c$, such that singlets do not move, and doublets move with a speed of roughly one eighth of the topological speed ($v_d/v_t \approx 0.125$), see Fig. 2.

In Fig. 3 we show a time sequence of microscope images showing the dynamics of the colloids. We distinguish single colloids (red) that are immobile from colloidal trains (green, cyan and yellow) consisting of one, two, and three doublets at the tail, and of one up to five single colloids at the front of the trains. The singlets and doublets in a train are well separated from each other by a primitive unit vector of the lattice. All trains move into the positive \mathbf{x} -direction with the doublets pushing the singlets. Nothing particular happens to the cyan train with

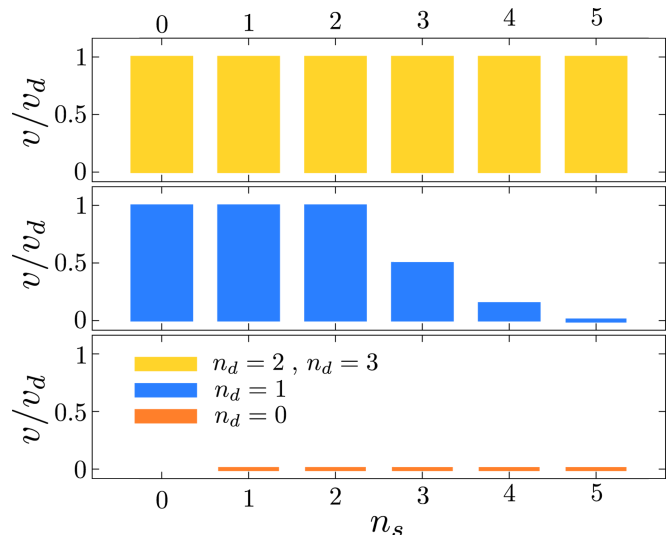


FIG. 4: Speed of the train (scaled with the speed of a doublet v_d) versus the load, i.e. the number of singlets in the train n_s . Data for different numbers of doublets in front of the train: $n_d = 0$ (orange), $n_d = 1$ (blue), $n_d = 2$ and 3 (yellow).

one doublet and one singlet moving through the field of view at the doublet speed v_d . The green train with one doublet and three singlets moves with half the doublet speed, Fig. 3(a-b), collects two further singlets, Fig. 3(c), and stalls, Fig. 3(d), until the two singlets close to the pushing doublets form a second doublet, Fig. 3(e). This increases the power of the train such that it resumes to move, Fig. 3(e-f) at the doublet speed. In Fig. 3(g) a third doublet is formed leaving only one singlet in the green train before it exits the field of view. Interestingly, when the green train passes the red singlets (sitting on

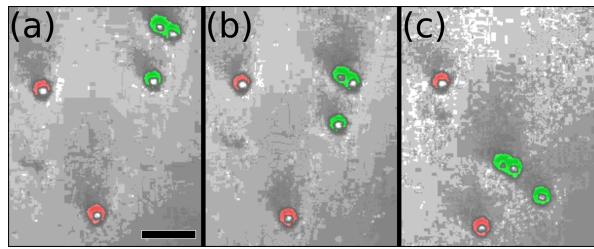


FIG. 5: Time sequence of microscope images showing a doublet (green) moving a singlet (green) out of its way. The other single colloids (red) remain at rest. Scale bar is $10 \mu\text{m}$. The images correspond to the times (a) $t = 0 \text{ s}$, (b) $t = 2 \text{ s}$, and (c) $t = 4 \text{ s}$. A video clip of the event recorded at twenty frames per second is provided in the supplemental material (adfig5.mp4).

the next track to the right) the front immobile red single colloid is mobilized and performs a single translation by one unit vector in the positive x -direction, compare the position of the red colloids next to the green train in Figs. 3(e) and 3(f). The yellow train originally consists of one doublet and two singlets, Fig. 3(a). It collects two further singlets, Figs. 3(b,c), and then moves as one doublet and four singlets train at a relatively slow speed $v \approx 0.15v_d$ through the image. No further doublets are formed from the singlets of the yellow train as it moves. In Fig. 4 we plot the speed of a train as a function of both the number of singlets in front of the train and the number of doublets at its tail. A train with no doublet is immobile and a train with more than one doublet can push up to five single colloids at the unloaded doublet speed. For one doublet we see a gradual transition from motion at the doublet speed v_d for trains with up to two singlets toward no motion for trains with five singlets.

Remarkably, none of the trains ever derails. This is due to the special properties of the confining colloidal potential which are inherited from the square pattern. In Fig. 5 we show the colloidal motion on a glass slide with no magnetic confining pattern. Doublets also move when performing a modulation loop without the magnetic pattern (albeit not by a unit vector) and singlets are generically at rest. However due to the absence of the confining potential, when one doublet moves onto a singlet, the singlet does not stay on track but is pushed to the side to let the doublet pass.

So far we have shown the coordinated motion of colloids in one direction. However, by changing the global orientation of the driving loop (winding around other fence points in \mathcal{C}) we can force the doublet to move along any of the four symmetry directions of the magnetic pattern. Hence, the doublet-induced motion of single colloids can potentially be used to arbitrarily set the position of the singlets across the pattern. A step in this direction is shown in Fig. 6 where a complex modulation loop is programmed to clean the surface of singlets.

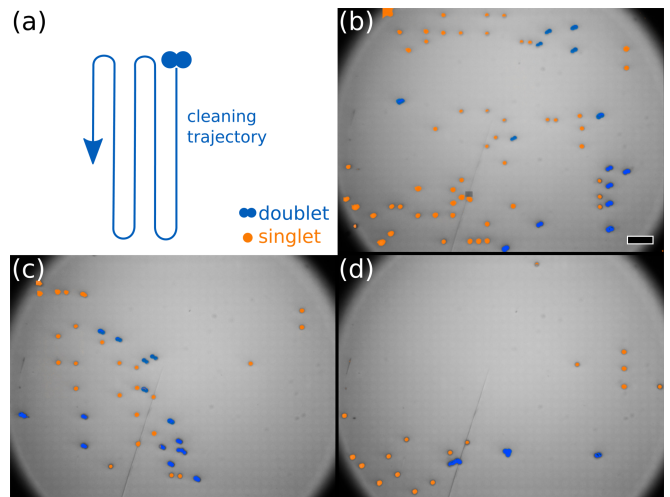


FIG. 6: Surface cleaning. (a) Schematic of the trajectory of a doublet. Sequence of microscope images showing the cleaning of an area from single colloids (orange) by meandering doublets (blue) taken at times $t = 0$ (b), $t = 2 \text{ min}$ (c), and $t = 6 \text{ min}$ (d). The scale bar is $20 \mu\text{m}$. A video clip of the event is provided in the supplemental material (adfig6.mp4).

Our colloidal trains are immersed into a low Reynolds number liquid where the propulsion of shape changing objects is governed by the area enclosed by the loop in shape space of the object [14, 15]. Swimmers are able to move by changing their shape. In contrast our biomimetic colloidal trains are driven by the shape of the potential created by the pattern and the external field which creates the topological nature of this classical non-adiabatic phenomenon. We have shown in references [8, 9, 16–20] that, like other classical topological transport phenomena [21–27], there exist similarities with quantum mechanical topological transport [28, 29].

We have demonstrated how long range many-body interactions between the well separated colloidal particles can help sustain the topological nature of the transport up to higher frequencies of driving. Such speeding up comes in handy for lab-on-the-chip applications such as transporting loads from one place of a chip to another. Whether the doublet-induced motion of the singlets is caused by direct superadiabatic non-equilibrium interparticle interactions [30] or mediated by hydrodynamic interactions constitutes the subject of future studies.

* Electronic address: Thomas.Fischer@uni-bayreuth.de

- [1] R. Dreyfus, J. Baudry, M. L. Roper, M. Fermigier, H. A. Stone, and J. Bibette, Microscopic artificial swimmers, *Nature* **437**, 862 (2005).
- [2] A. Snezhko, M. Belkin, I. S. Aranson, and W. K. Kwok, Self-Assembled Magnetic Surface Swimmers, *Phys. Rev. Lett.* **102**, 118103 (2009).

- [3] K. J. Solis, and J. E. Martin, Chevrons, filaments, spinning clusters and phase coexistence: emergent dynamics of 2- and 3-d particle suspensions driven by multiaxial magnetic fields, *Soft Matter* **13**, 5676 (2017).
- [4] C. Bechinger, R. Di Leonardo, H. Löwen, C. Reichhardt, G. Volpe, and G. Volpe, Active particles in complex and crowded environments, *Rev. Mod. Phys.* **88**, 045006 (2016).
- [5] F. E. Fish, Kinematics of ducklings swimming in formation - consequences of position, *J. Exp Zoology* **273**, 1 (1995).
- [6] A. Snezhko, I. S. Aranson, Magnetic manipulation of self-assembled colloidal asters, *Nat. Matter.* **10**, 698 (2011).
- [7] N. Casic, N. Quintero, R. Alvarez-Nodarse, F. G. Mertens, L. Jibuti, W. Zimmermann, and T. M. Fischer, Propulsion efficiency of a dynamic self-assembled helical ribbon, *Phys. Rev. Lett.* **110**, 168302 (2013).
- [8] D. de las Heras, J. Loehr, M. Lönne, and Th. M. Fischer, Topologically protected colloidal transport above a square magnetic lattice, *New J. Phys.* **18**, 105009. (2016).
- [9] J. Loehr, D. de las Heras, M. Lönne, J. Bugase, A. Jarosz, M. Urbaniak, F. Stobiecki, A. Tomita, R. Huhnstock, I. Koch, A. Ehresmann, D. Holzinger, and Th. M. Fischer, Lattice symmetries and the topologically protected transport of colloidal particles, *Soft Matter* **13**, 5044 (2017).
- [10] C. Chappert, H. Bernas, J. Ferré, V. Kottler, J.-P. Jamet, Y. Chen, E. Cambri, T. De-Volder, F. Rousseaux, V. Mathet, and H. Launois, Planar patterned magnetic media obtained by ion irradiation, *Science* **280**, 1919 (1998).
- [11] P. Kuświk, A. Ehresmann, M. Tekielak, B. Szymański, I. Sveklo, P. Mazalski, D. Engel, J. Kisielewski, D. Lenge-mann, M. Urbaniak, C. Schmidt, A. Maziewski, and F. Stobiecki, Colloidal domain lithography for regularly arranged artificial magnetic out-of-plane monodomains in Au/Co/Au layers, *Nanotechnology* **22**, 095302 (2011).
- [12] R. Adler, A study of locking phenomena in oscillators, *Proceedings of the I.R.E. and Waves and Electrons*, **34**, 351 (1946).
- [13] The drag force on a train of N spheres of radius r scales as $Nr/\ln(N)$. See e.g. J. Happel and H. Brenner, *Low Reynolds number hydrodynamics*, Martinus Nijhoff Publishers, page 156 (1983).
- [14] A. Shapere, and F. Wilczek, Geometry of self-propulsion at low Reynolds number. *J. Fluid Mech.*, **198**, 557 (1989).
- [15] A. Shapere, and F. Wilczek, Efficiency of self-propulsion at low Reynolds number, *J. Fluid Mech.*, **198**, 587 (1989).
- [16] J. Loehr, M. Lönne, A. Ernst, D. de las Heras, and Th. M. Fischer, Topological protection of multiparticle dissipative transport, *Nat. Comm.* **7**, 11745 (2016).
- [17] A. M. E. B. Rossi, J. Bugase, and Th. M. Fischer, Macroscopic Floquet topological crystalline steel and superconductor pump, *Eur. Phys. Lett.* **119**, 40001 (2017).
- [18] A. M. E. B. Rossi, J. Bugase, T. Lachner, A. Ernst, D. de las Heras, and Th. M. Fischer, Hard topological versus soft geometrical magnetic particle transport, *Soft Matter* **15**, 8543 (2019).
- [19] H. Massana-Cid, A. Ernst, D. de las Heras, A. Jarosz, M. Urbaniak, F. Stobiecki, A. Tomita, R. Huhnstock, I. Koch, A. Ehresmann, D. Holzinger, and Th. M. Fischer, Edge transport at the boundary between topologically equivalent lattices, *Soft Matter* **15** 1539 (2019).
- [20] J. Loehr, D. de las Heras, A. Jarosz, M. Urbaniak, F. Stobiecki, A. Tomita, R. Huhnstock, I. Koch, A. Ehresmann, D. Holzinger, and Th. M. Fischer, Colloidal topological insulators, *Comm. Phys.* **1**, 4 (2018).
- [21] M. C. Rechtsman, J. M. Zeuner, Y. Plotnik, Y. Lumer, D. Podolsky, F. Dreisow, S. Nolte, M. Segev, and A. Szameit, Photonic Floquet topological insulators, *Nature* **496**, 196-200 (2013).
- [22] M. Xiao, G. Ma, Z. Yang, P. Sheng, Z.Q. Zhang, and C.T. Chan, Geometric phase and band inversion in periodic acoustic systems, *Nat. Phys.* **11**, 240 (2015).
- [23] A. Murugan and S. Vaikuntanathan, Topologically protected modes in non-equilibrium stochastic systems, *Nat. Comm.* **8**, 13881 (2017).
- [24] C. L. Kane, and T. C. Lubensky, Topological boundary modes in isostatic lattices, *Nat. Phys.* **10**, 39 (2014).
- [25] J. Paulose, B. G. Chen, and V. Vitelli, Topological modes bound to dislocations in mechanical metamaterials, *Nat. Phys.* **11**, 153 (2015).
- [26] L. M. Nash, D. Kleckner, A. Read, V. Vitelli, Ari M. Turner, and W. T. M. Irvine, Topological mechanics of gyroscopic metamaterials, *Proc. Nat. Acad. Sci.* **112**, 14495 (2015).
- [27] S. D. Huber, Topological mechanics, *Nat. Phys.* **12**, 621 (2016).
- [28] M. Z. Hasan, and C. L. Kane, Colloquium: Topological insulators, *Rev. Mod. Phys.* **82**, 3045 (2010).
- [29] S-Q. Shen, *Topological insulators: Dirac equation in condensed matters*, Springer Science, and Business Media (2013).
- [30] M. Schmidt and J. M. Brader, Power functional theory for Brownian dynamics, *J. Chem. Phys.* **138**, 214101 (2013).